Simulation of wear in hydraulic percussion units using a co-simulation approach

Håkan Andersson, Joakim Holmberg, Kjell Simonsson, Daniel Hilding, Mikael Schill and Daniel Leidermark

This is an electronic version of an article published in:
Andersson, H., Holmberg, J., Simonsson, K., Hilding, D., Schill, M., Leidermark, D., (2022), Simulation of wear in hydraulic percussion units using a co-simulation approach, *International Journal of Modelling and Simulation*, , 1-17. https://doi.org/10.1080/02286203.2022.2066349

Original publication available at:
https://doi.org/10.1080/02286203.2022.2066349

RESEARCH ARTICLE

Simulation of wear in hydraulic percussion units using a co-simulation approach

H. Andersson[a,b], L. J. Holmberg[b], K. Simonsson[b], D. Hilding[c], M. Schill[c], D. Leidermark[b]

[a]Epiroc, Tools & Attachments Division, Dragonvägen 2, 391 27 Kalmar, Sweden; [b]Division of Solid Mechanics, Linköping University, 581 83 Linköping, Sweden; [c]Dynamore Nordic AB, Brigadgatan 5, 587 58 Linköping, Sweden

ARTICLE HISTORY
Compiled April 29, 2022

ABSTRACT
In this study, a developed co-simulation method, which couples 1D-fluid and 3D-structural models, has been utilised to simulate wear in a hydraulic percussion unit. The effect of wear is generally detrimental on performance and lifetime for such units, but can also cause catastrophic failure and breakdown, requiring a total overhaul and replacement of core components. One experiment of standard straight impact was performed to investigate the tolerance against seizure. The percussion unit was operated at successively increasing operating pressures, and the level of wear was registered at each step, until seizure occurred. The co-simulation model was used to replicate the running conditions from the experiment to simulate the structural response to be used as input for the wear routine to calculate the wear depth. The wear pattern from the simulations corresponds well to the wear pattern from the experiment. Further, the effect of a misaligned impact on wear development was also studied, as this is a loading situation that typically occurs for hydraulic percussion units. The study demonstrates that the simulation method used has a potential for simulating wear and predicting seizure in hydraulic percussion units.

KEYWORDS
Co-simulation; Fluid-structure coupling; System simulation; FEM; Wear; Fluid power machinery; Seizure

1. Introduction

The effects of wear and seizure in hydraulic percussion units may have a significant impact on performance and lifetime of core components. Damages from wear can result in a wide range of different scenarios, which may vary from a minor increase in oil leakage to a complete breakdown, where the latter often requires an entire overhaul and replacement of core components. The risk for seizure in new designs of hydraulic percussion units is nowadays mainly evaluated on physical prototypes, which demands a lot of time and resources. Therefore, there is a strong incentive to develop simulation tools that make it possible to simulate wear and to predict seizure in such units.

Hydraulic percussion units are found in hydraulic hammers and rock drills, which are used e.g. for demolishing concrete structures in the construction industry, see e.g.

CONTACT H. Andersson. Email: hakan.andersson@epiroc.com

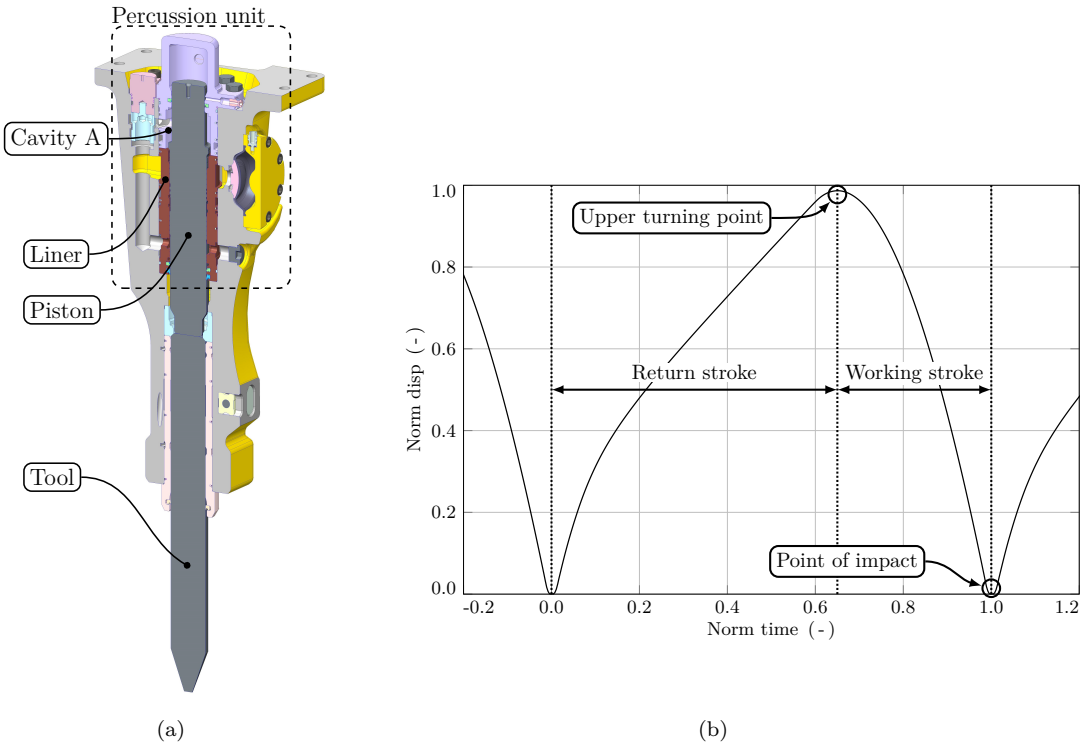

(a) (b)

Figure 1. (a) some components and features in the percussion unit of a hydraulic hammer, and (b) a typical piston movement for the working cycle for a hydraulic percussion unit.

Park and Kim [1], or for drilling blast holes in hard rock in the mining industry, see e.g. Lundberg [2]. These types of hard materials require high impact forces to be fragmented and the main feature of the percussion unit is specifically its ability to generate high impact forces. Figure 1 shows a typical percussion unit in a hydraulic hammer, and its working cycle. The key component to generate high impact forces is the piston, which will follow a percussive movement by repeatedly switching the pressure in cavity A. A stress wave in the tool will be generated at each impact, which will be transferred to its tip to fragmentise the material. A more detailed description of the percussion unit can be found in e.g. Giuffrida and Laforgia [3].

In order to simulate wear in percussion units it is crucial to capture the lateral behaviour of the piston and the liner, since wear only happens when contact occurs between the components. This behaviour is to a large extent controlled by the fluid film that is formed between these components, and the viscous squeeze damping effect that occurs when the components are moving toward each other. The damages can be initiated by fundamental features such as length or diameter of the piston and the liner in the percussion units, or by local ones such as sharp edges and corners where burrs often exist. Seizure damages may be of many different types, from simple small scratches that will not affect the product performance at all, to severe damages that make the piston stick to the liner. Small scratches may generate oil leakage but will probably not have any major effect on performance or lifetime. Medium sized damages will often grow and eventually cause major breakdown. If seizure occurs during the physical prototype test and verification phase in the product development process, an extensive re-design must be initiated, which in turn will require further testing. Therefore, it is important that the risk of seizure and wear damage is minimised early

in the product development process, and a simulation tool that facilitates such analyses on virtual prototypes would be of great interest for the industry.

Studies of wear using the Finite Element (FE) method started in the nineteen-eighties, where the work by Ohmae and Tsukizoe [4] was among the first ones published. The authors analysed the wear process associated to the relative sliding of two aluminium blocks. No wear law was utilised to determine the effect of wear, but an elasto-plastic material model was used, and wear was assumed to occur at the zones where the material had been loaded above the plastic limit. Põdra et al. [5] studied the wear process from a conformal conical spinning contact situation. In that study, the wear process was analysed based on the pressure on the contact surfaces, where a wear law of an Archard type [6] was used to estimate the wear depth. In the work by Borrvall et al. [7], functionalities to study different wear processes, such as wear of machine components or forming tools, were implemented in the FE-software LS-DYNA [8]. A study of the wear process of machinery components in buildings was performed by Puryear et al. [9] using wear routines in LS-DYNA along with an Archard [6] type wear law. The wear depths for complete service lives were calculated for three material combinations, from which the combination with the longest life was chosen. In the work of Hatam and Khalkhali [10] the wear of a brake pad for a hydraulic disc brake system was analysed by the use of the Archard's wear law in an FE-context. To the best of the authors knowledge, no study involving simulation of wear in hydraulic percussion units has been published.

In this paper, one experiment was conducted on a hydraulic percussion unit with the objective to investigate the relation between the operating pressure and the type of wear. The setup from the experiment was replicated by a simulation model of the percussion unit that uses the previously developed co-simulation approach by Andersson et al. [11–14], where the wear on the contact surfaces of the piston and the liner was evaluated using the wear routines in LS-DYNA.

The intention was not to simulate absolute values of wear depth, but rather to predict wear patterns and to identify areas with high risk for seizure. Such a procedure will be useful in the design phase, and ultimately reduce the need for testing physical of prototypes.

2. Experiment

The resistance against wear and seizure in a hydraulic percussion unit at standard impacting condition, i.e. the piston and the tool are aligned in parallel, were investigated by conducting an experiment where the operating pressure was successively increased until seizure was registered. A standard Epiroc SB202 hydraulic hammer was used in the experiment and the measurement setup is shown in Figure 2, see Andersson et al. [13] for details on the measurement configuration.

The key components in this experiment were the piston and the liner, which were manufactured while controlling critical measures to achieve a specific radial clearance, see Figure 3 for the components (highlighted) that were in focus in this experiment, i.e. the piston and the liner, cavity A marked in blue, and cavity C marked in green.

The pressure in cavity A, p_{A}, acts on the top side of the piston and on the inside of the liner, while the pressure in cavity C, p_{C}, is acting on the outside of the liner. The pressure in cavity A was registered by a pressure sensor that was connected directly to the cavity, see Figure 2. The pressure in cavity C is almost equal to the operating pressure of the hammer, which was registered by measurement during the experiment,

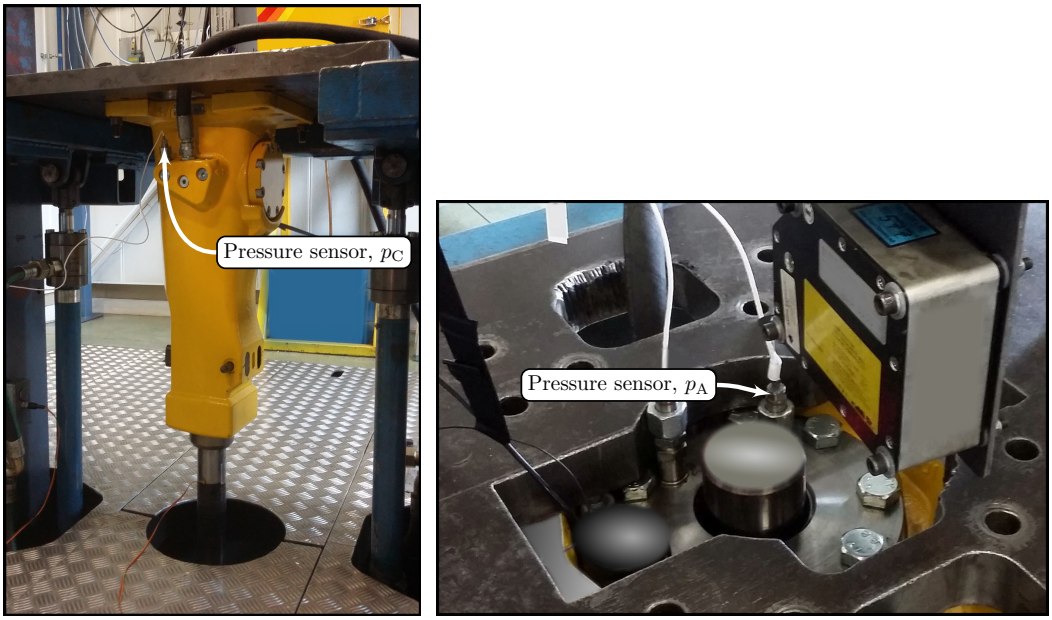

(a) (b)

Figure 2. The test rig and the hydraulic hammer setup used in the experiment. The sensor for pressure p_C was located on the left side of the hammer (a) and the sensor for p_A was located on the upper side of the hammer (b).

and was used as an approximation of the pressure in cavity C in the modelling part of this study. The pressure in these cavities defines the resulting pressure Δp, which is the pressure difference acting on the upper part of the liner and is calculated as

$$\Delta p = p_C - p_A. \tag{1}$$

The characteristic behaviour of the pressures p_C and p_A are shown in Figure 4, which also shows the evaluation of Δp and when its maximum magnitude occurs.

Since the working principle of the percussion unit is based on an alternating pressure in cavity A, the upper part of the liner will be subjected to a high resulting pressure during the return stroke, i.e. p_A = low and p_C = high. The pressure load on the liner will generate a radial deformation of the liner that will decrease the gap between the liner and the piston, and at a specific load contact will occur between the components. The magnitude of this load is depending on the structural stiffness of the liner, the radial clearance between the piston and the liner, and the fluid film that is formed between the components.

The experiment was divided into separate sequences, where the operating pressure, henceforth the pressure p_C, was increased for each sequence. For each sequence the operating pressure was pre-set according to Table 1 before the percussion unit was started, which then was in operation for approximately 5 seconds before shutdown. The unit was then disassembled and the piston and the liner were visually inspected and critical regions of the components were documented. As long as no seizure could be observed, the experiment was continued using the same components, where the unit was assembled and set up as in the previous sequence. The operating pressure was increased one step, and the next sequence was started. This procedure was repeated

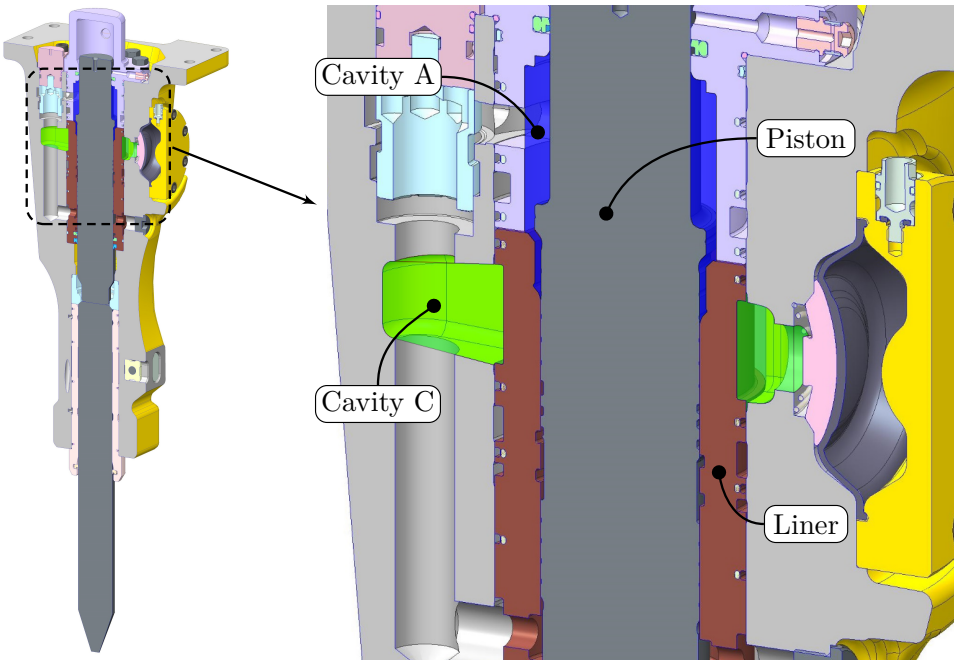

Figure 3. Details of the hydraulic percussion unit showing the cavities A (transparent blue) and C (transparent green) on the inside and on the outside of the liner respectively.

until seizure was registered, which happened to occur after five sequences for the component combination used in this experiment. For another combination, seizure might occur at a different operating pressure level due to variation in several of the critical parameters which are mentioned above. The running conditions and results from each sequence of the experiment are presented in Table 1 and Section 4, all values are normalised with respect to running condition 5. Further, the pressure $\overline{p}_{\mathrm{C}}$ refers to the average value for the complete running cycle during the respective sequence.

Table 1. Normalised parameters and wear results from the experiment.

Running condition	$\overline{p}_{\mathrm{C}}$ (-)	Max Δp (-)	Result
1	0.69	0.69	No wear
2	0.78	0.80	No wear
3	0.89	0.91	Polished
4	0.92	0.91	Polished
5	1.0	1.0	Seizure

3. Wear and Simulations

The previously developed co-simulation method by Andersson et al. [11–14] was utilised to simulate wear in hydraulic percussion units, and more specifically the experimental setup described in the above experimental section. A flow chart of the simulation approach is illustrated in Figure 5, where the co-simulation interface was implemented by an Functional Mock-up Unit (FMU), following the Functional Mock-up Interface (FMI) standard [15]. In this figure, the incorporation of the wear features

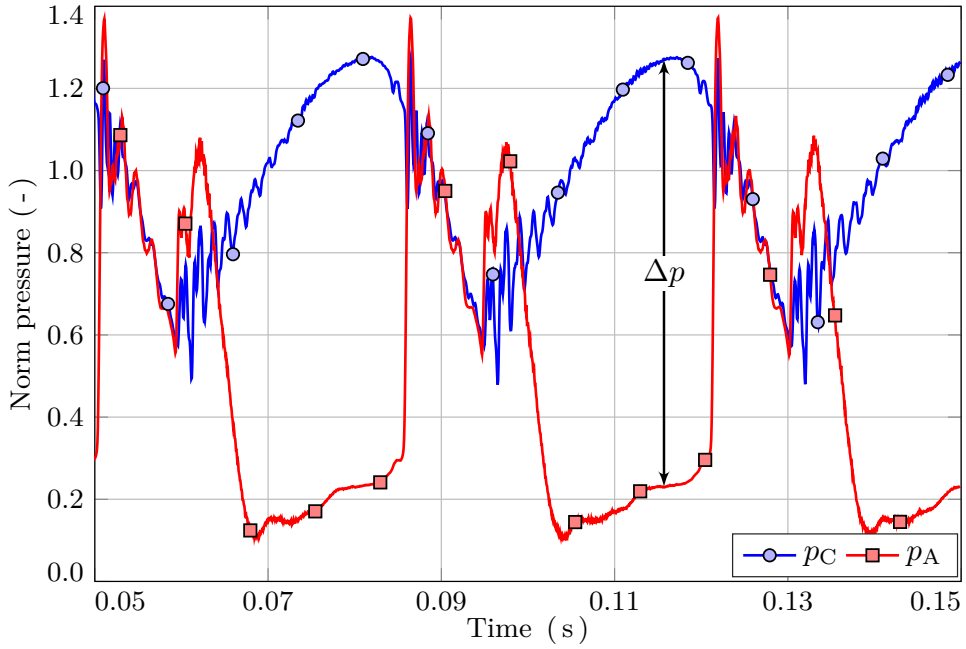

Figure 4. The typical pressure characteristic in cavity A (red curve) and in cavity C (blue curve). The definition of the pressure difference Δp is also shown.

in the simulation tool is new, which facilitates simulation of wear processes from general FE-results. In this methodology LS-DYNA has been utilised for the simulation of the structure deformation, part interaction through contacts, and the simulation of wear as described in this work. Furthermore, the simulation of the fluid parts in the tool was described by using Hopsan [16].

3.1. Wear

Wear is often classified in three different types, abrasive, erosive and adhesive. Abrasive wear occurs when particles come into contact with solid material, which is then removed. The mechanism of erosive wear is similar but instead of particles it is a fluid that generates the erosion. Cavitation is also classified as erosive wear caused by collapsing bubbles in a fluid, which generates high pressure peaks and by that removes material from a solid component. However, the type of wear in focus in this study is the adhesive wear due to sliding interfaces between components of metallic material in the hydraulic percussion unit. A more comprehensive description of different wear processes can be found in e.g. Hutchings and Shipway [17].

Adhesive wear, also known as sliding wear, occurs when two different components come into contact during sliding and material is transferred between them. The main process of adhesive wear can be divided into three stages, which is schematically illustrated in Figure 6 for a material combination of different hardness, where the lower material being the softer one.

The process starts when two asperities come into contact during sliding, see stage I in Figure 6, which may occur at high loads or when the lubrication film breaks down. As the sliding progresses in stage II, the lower material will adhere to the upper part by local welding. Further, the lower material undergoes plastic deformation and

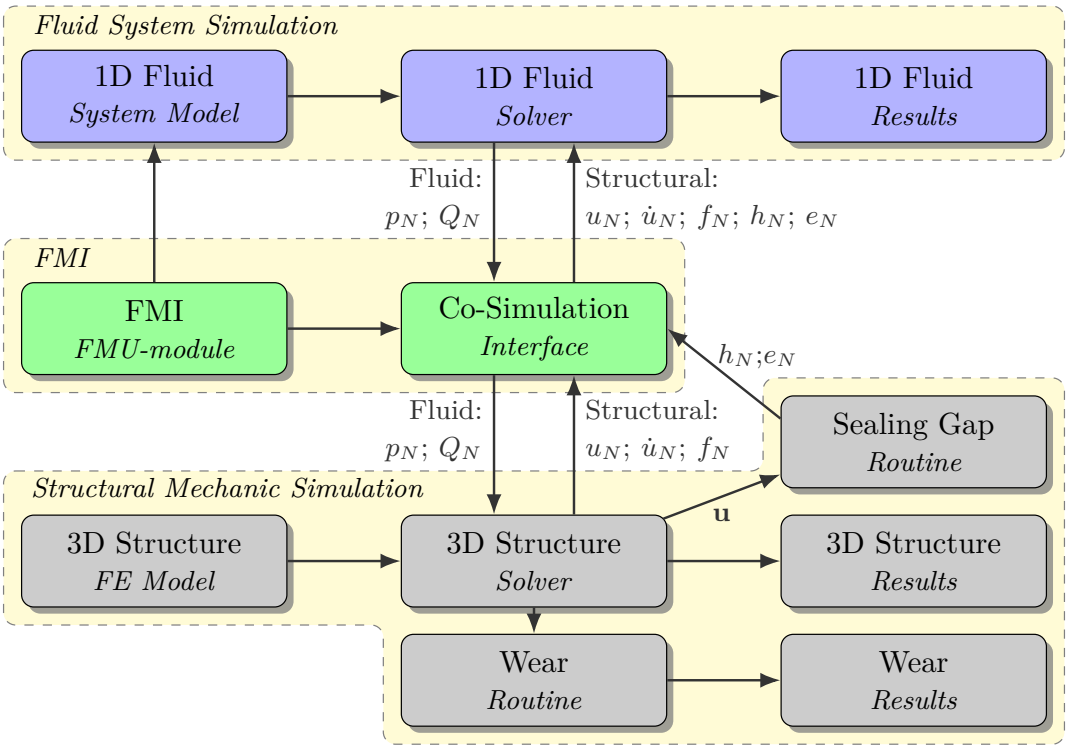

Figure 5. The overall simulation sequence. The new functionalities defined in this study are related to the Wear features.

shear cracks will be initiated and propagate along the dotted line in Figure 6. The last phase concludes the process, i.e. stage III, where a small piece of the softer material is sheared off and has been transferred to the harder material.

Adhesive wear is controlled by many different parameters and processes, such as e.g. hardness, surface roughness, contact force, temperature, chemistry and lubrication. Hutchings and Shipway [17] also use the terms scuffing, scoring and galling, which are more specific descriptions of the present adhesive wear process. It is probably possible to find that both scuffing and galling are causing wear in the percussion unit, but scoring requires hard particles to be present in the sliding wear region causing grooves and scratches, and this should be rare.

Scuffing and galling occurs when the oil film breaks down, and an inadequately lubricated contact situation occurs. Scuffing mainly depends on the chemistry of the lubrication and the microstructure and the properties of the contact surfaces, and it occurs when the temperatures of these surfaces have reached a critical value. At the elevated temperature, the viscosity of the lubricant will locally decrease and eventually break down. This will significantly lower the load carrying capacity of the lubricant. Galling is often referred to as a more severe form of scuffing and will generate larger surface damages and transfer of larger pieces of materials due to local welding. When adhesive wear occurs it is often hard to find one single root cause, but it is often a consequence of several different parameters, as has already been mentioned. An example of seizure in a percussion unit is shown in Figure 7. Due to this complex nature, many of the existing predictive wear laws have been developed using specific experiments to achieve a quantitative prediction of wear. A frequently used theory to describe the mechanism of adhesive wear is the theory presented by Archard [6], where

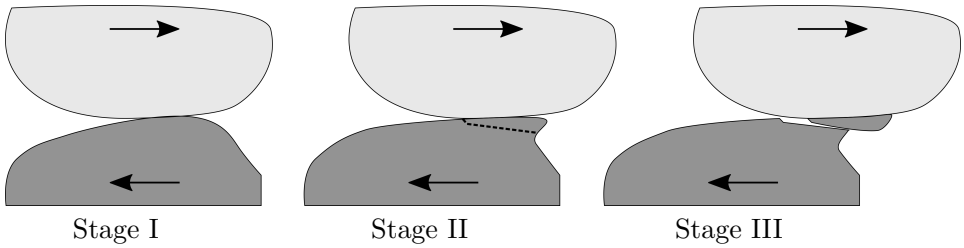

Figure 6. A schematic illustration of the three adhesive wear process stages at an asperity contact situation.

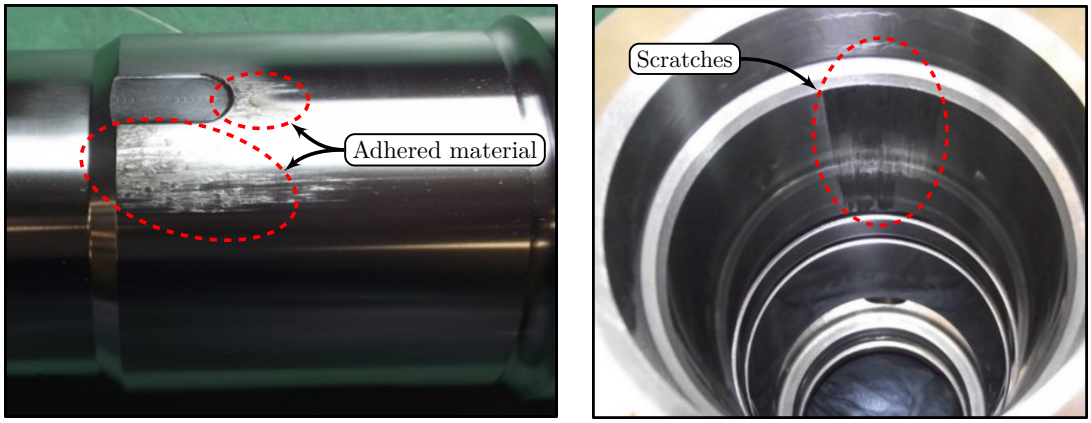

Figure 7. An example of adhesive wear in a hydraulic percussion unit that has resulted in seizure. Material has been transferred to the piston (a) from the liner (b) by an adhesive wear process.

the main findings are that the wear rate is proportional to the load, sliding distance and surface hardness. Furthermore, it was found to be independent of the contact area and the sliding speed. This wear law may be expressed according to

$$V = k\, s \frac{W}{H} \tag{2}$$

where V is the total volume of the wear debris, k is the wear coefficient, s is the sliding distance, W is the load and H is the hardness of the softer material. The wear coefficient will be different for each contact situation, and is mainly dependent of the type of lubrication, surface roughness and material combination.

3.2. Simulation of wear

In this study, the approach to simulate wear in a hydraulic percussion unit consists of one system model for the fluid system of the percussion unit represented by Hopsan [16], and one FE-model representing the structural parts of the unit. The simulation model is based on the one used in the previous work by Andersson et al. [14], where all specific details can be found, and has here been further developed to incorporate wear routines for the simulation of wear. These developments are completely related to the structural FE-model, and are described in this section. No modifica-

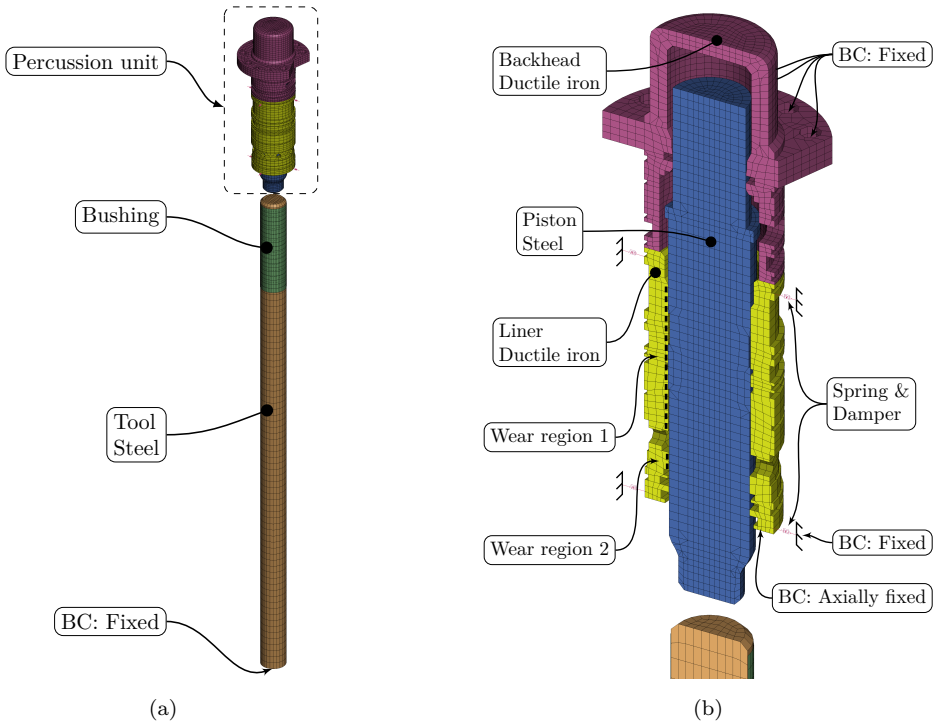

Figure 8. The complete FE-model (a), and the details of the percussion unit and the wear regions (b). The type of material for each component is defined, and the labels named BC represents the model boundary conditions.

tions of the fluid system model were needed, except for some changes of initial and inlet pressures to reach the same running conditions as in the experiment. Figure 8 displays the FE-model with applied boundary conditions and materials. Moreover, a mechanical Mortar contact condition is present between the piston and the liner, at wear regions 1 and 2.

To facilitate simulation of wear mechanisms for complex geometries, an Archard-type wear law is implemented in LS-DYNA [7]. In this implementation the wear rate $\dot{w}$ is in the form of wear depth per time unit with the dimension m/s, and is calculated according to

$$\dot{w} = k\frac{p\dot{d}}{H} \tag{3}$$

where p is the contact pressure and $\dot{d}$ is the sliding speed. This calculation is performed for each surface, where the hardness for each surface is specified. The wear routines in LS-DYNA are based on an uncoupled simulation, and the wear depth and the sliding distance are calculated as independent variables. Two regions between the piston and the liner were defined to accommodate wear, where a mechanical Mortar contact is utilised, see wear region 1 and 2 in Figure 8b. To simulate wear in LS-DYNA, the keyword CONTACT_ADD_WEAR was used. This keyword defines the input to the wear calculation of the Archard type wear law which are the contact region, the wear constant and the hardness for each material. Here, a wear coefficient of 0.002 was used, and the hardness for the steel material and the ductile iron material were normalised by the steel material to unity and 0.488, respectively.

Five different simulation cases were configured and carried out, representing each of the running conditions in the experiment, i.e. simulation case 1 represents the experimental running condition 1 and so on. In contrast to the experiment, the wear simulations were performed on virgin material, i.e. each simulation case started without any previous wear damage. The initial pressure for all cavities connected to the high pressure side in the percussion unit were set to 18.5 MPa for case 1–3 and 22.5 MPa for case 4–5. The initial pressure for all cavities belonging to the low pressure side was set to 0.3 MPa for all cases. The pressure relief valve on the inlet side was utilised to reach the registered average operating pressure for each running condition in the experiment, see Table 1. The orifice diameter of the restrictor on the outlet was adjusted to meet the impact frequency for each running condition. The piston reaches a steady state operation after one cycle.

A computational server was utilised to run the simulations, and both the FE and the system simulation were run on the same physical computer. This server has the following specification, four Intel Xeon Gold 6146 (3.2 GHz, 12 core) CPUs, 288 GB RAM, and with the operating system Window Server 2016 Standard (64-bit). Four processor cores with shared memory were used for the LS-DYNA simulation and one core for the Hopsan simulation. The total simulated time was 0.17 s, which was enough to complete four working cycles at steady state conditions for the percussion unit. The clock time spent to complete one simulation was ≈13.5 h, where the simulation of contacts required the most resources, ≈60%.

4. Results and discussion

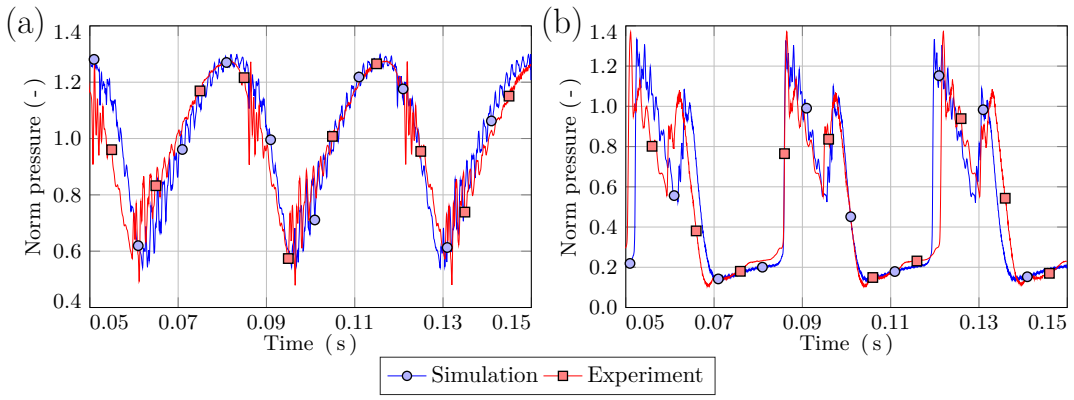

Figure 9. Inlet pressure for case 4, simulated and experiment for (a) cavity C, and (b) cavity A.

In Figure 9 the pressure in cavity C and A are compared for the simulation case 4 and for the running condition 4 in the experiment, to validate the simulation model. A good agreement between experiments and simulations can be concluded from these figures, except from a small difference for the impact frequency, ≈1%. The signals were synchronised at $t = 0.086$ s to clarify the differences in-between, and a comparison concludes that the discrepancy in amplitude is negligible. Not only is the overall character in the pressure signals from the experiment well represented, but also short duration events are found to agree to a high degree. The agreement of pressure signals indicates that the simulation model represents the real mechanisms of the hydraulic

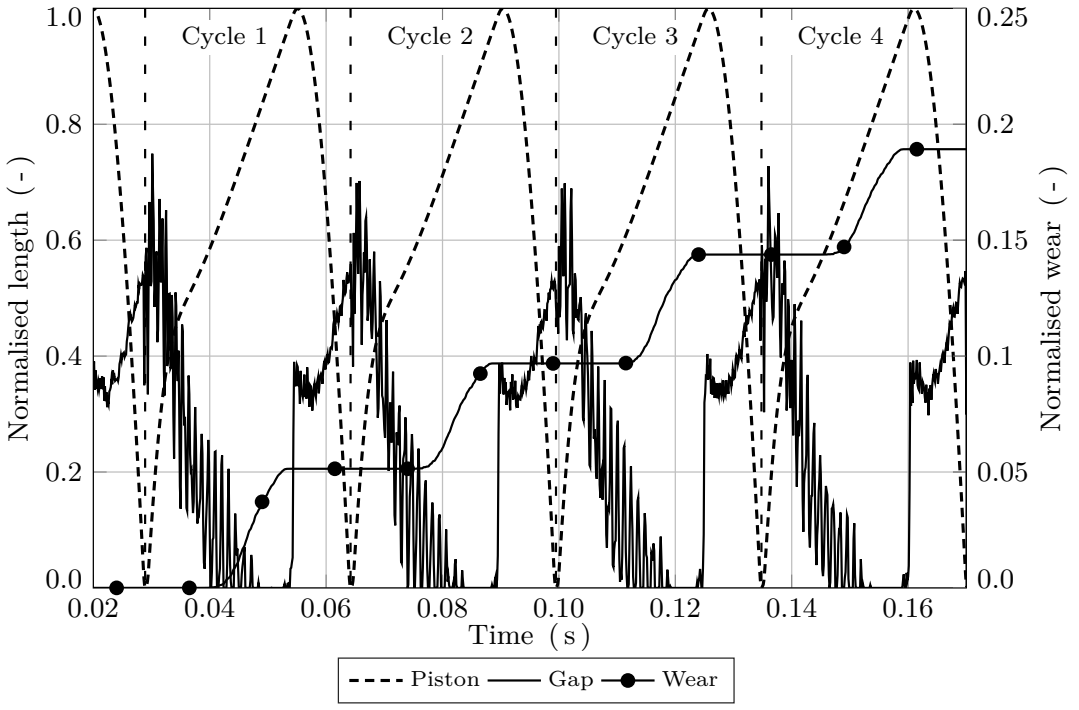

Figure 10. The piston position, the gap distance, and the accumulated wear for case 4. The vertical dashed lines show the time of impact and the interval in-between are defining each working cycle. The ordinate values of the normalised piston position and the gap height are displayed on the left y-axis, while the values for the normalised wear depth is shown on the right y-axis.

percussion unit, which is in-line with the overall conclusion from the previous work on validation of the co-simulation tool, see Andersson et al. [13].

The simulated overall wear process for the maximum wear depth representing running condition 4 in the experiment is shown in Figure 10. This figure shows that the wear occurs during the return stroke, i.e. when the pressure in cavity A, p_{A}, is low and the pressure difference Δp is high. At this phase of the working cycle, the high pressure load must be handled by the structural strength of the liner to prevent contact with the piston. The normalised data for the gap height for the node of the maximum wear depth, see the curve Gap in Figure 10, and the piston positions are also displayed. The gap height was normalised as the quotient between the simulated gap height and the actual clearance C between the piston and the liner used in the experiment as

$$\text{Norm } h = \frac{h}{C}. \tag{4}$$

From this curve it is obvious that wear occurs when the gap height approaches zero, or is equal to zero. The overall average value of the stroke length for all four working cycles $\overline{\Delta u}_{\mathrm{p}}$ was calculated according to

$$\overline{\Delta u}_{\mathrm{p}} = \frac{1}{m}\sum_{n=1}^{m}\left(\mathrm{Max}\left(u_{\mathrm{p}_n}\right) - \mathrm{Min}\left(u_{\mathrm{p}_n}\right)\right) \tag{5}$$

where $\mathrm{Max}\left(u_{\mathrm{p}_n}\right)$ is the maximum piston position for the working cycle n, $\mathrm{Min}\left(u_{\mathrm{p}_n}\right)$ is

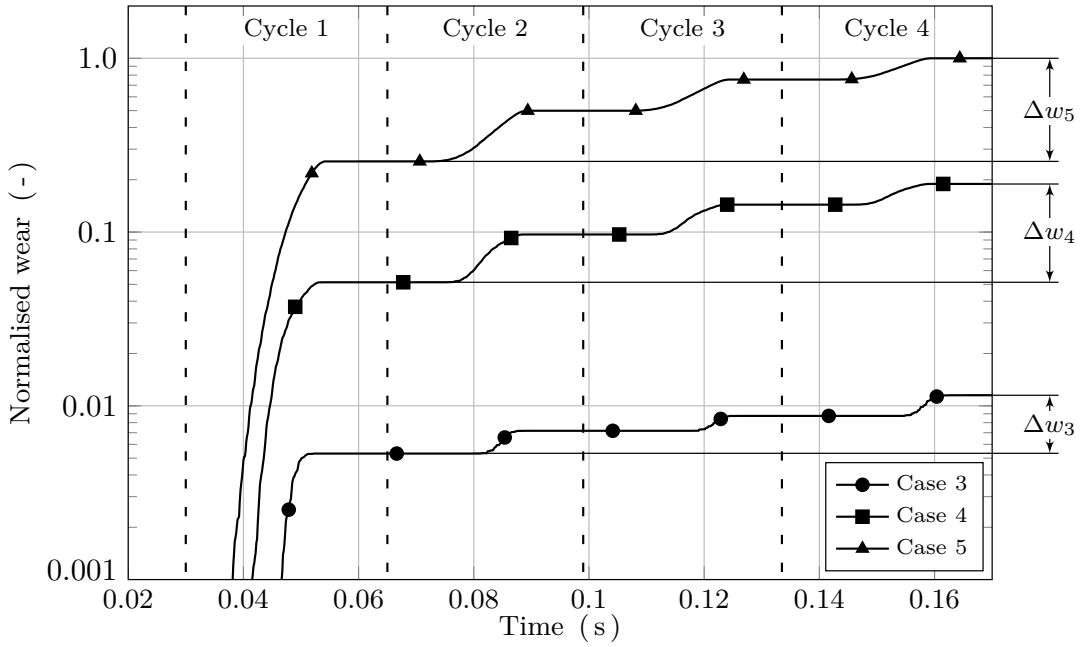

Figure 11. The normalised accumulated wear for the three simulations for the node on the liner where the maximum wear depth was registered. Note the logarithmic scale on the y-axis.

the minimum piston position for the same cycle, and m is the number of working cycles taken into account. The normalised piston position was calculated as the quotient between the piston position u_p and the overall average stroke length, see Eq. 5, for all four working cycles according to

$$\text{Norm } u_\mathrm{p} = \frac{u_\mathrm{p}}{\overline{\Delta u_\mathrm{p}}} \tag{6}$$

which is shown in the curve Piston in Figure 10. The tool impact is represented in Figure 10 by the Norm $u_\mathrm{p} = 0$, which also is marked by the vertical dashed lines in the figure, and the upper turning point at Norm $u_\mathrm{p} = 1$. The working cycle is defined as the time interval between each impact.

The normalised accumulated wear depth for the three damaged cases are shown in a logarithmic scale for comparative reasons in Figure 11, which also displays the accumulated wear in relation to the working cycles. Here, the final wear depth for case 5 was set to unity, to represent seizure, and the wear depth for case 3 and 4 were normalised against the results from case 5 as

$$\text{Norm } w_n = \frac{w_n}{w_5} \tag{7}$$

where the index n represents the simulation case. Figure 11 also shows that the wear rate for each working cycle are approximately equal. The difference in the final wear depth for each case are almost one order of magnitude. This result also justifies the simulation procedure of ignoring the initial wear depth from the previous simulation case since the final wear depth for each case is lower than the wear depth for the initial cycle for the following case. Furthermore, the intention of the study is not to generate

absolute predictions of the wear depth, but the aim is rather to identify an indicative measure when seizure is initiated. Results from the experiments and the simulations are shown in Table 2.
Furthermore, the wear/cycle were calculated from the wear depth for the working cycles 2–4 as

$$\text{Wear/cycle} = \frac{\Delta w_n}{3} \tag{8}$$

where Δw_n were extracted as in Figure 11.

Wear results are shown in Figure 12 for the liner from the experiment and the simulations compared for the cases that did show wear. The wear results from the experiment are represented by photographs, showing the affected inner surfaces at the top of the liner, i.e. wear region 1, see Figure 8b. The results from the simulations are shown as fringe plots of nodal results of normalised wear depth on the contact surfaces. The photographs of the liner show that the contact surfaces are polished to a certain degree, and for running condition 5 in the experiment scratches indicate that seizure occurs. The scratches indicate that adhesive wear is present, but the specific wear process, scoring, scuffing or galling, was not determined in this study.

The normalised gap Norm h_n was evaluated as the quotient between the simulated gap h_n and the gap between the unloaded components used in the experiment h_{Exp}, according to

$$\text{Norm } h_n = \frac{h_n}{h_{\text{Exp}}} \tag{9}$$

where the subscript n is representing the simulation case. For running condition 1 and 2 in the experiment, no wear could be identified, which also was the result from the simulations. The simulations indicate a minimum normalised gap between contact surfaces of 11.0% and 3.3% for running condition 1 and 2 in the experiment respectively, and obviously no wear occurs because there is no contact. For the other cases, i.e. case 3–5, the minimum normalised gap was equal to zero, which indicate contact. These results are in line with the observations from the experiment, which shows obvious signs that contact has occurred, see Figure 12. The polished surfaces may be classified as a low degree of wear. From the pictures of the liner in Figure 12a and b, it could be noticed that slightly more material is removed in case 4 and the area of the contact surfaces are somewhat larger. The simulations of the cases 3 and 4 show that the normalised wear/cycle for the liner increases from 0.0021 to 0.046, see Table 2, i.e. $\approx$22 times larger. The simulated wear of the liner, see Figure 12, is indicating that the maximum wear depth is located at the top of the inside surface, and the magnitude declines when the results further down are examined. Similar patterns could also be

Table 2. Experimental results and normalised wear depth from the simulations.

Case	Experimental Wear Result	Liner Wear/cycle	Piston Wear/cycle	Min gap (%)
1	No	0	0	11.0
2	No	0	0	3.3
3	Polished	0.0021	0.0009	0
4	Polished	0.046	0.019	0
5	Seizure	0.248	0.082	0

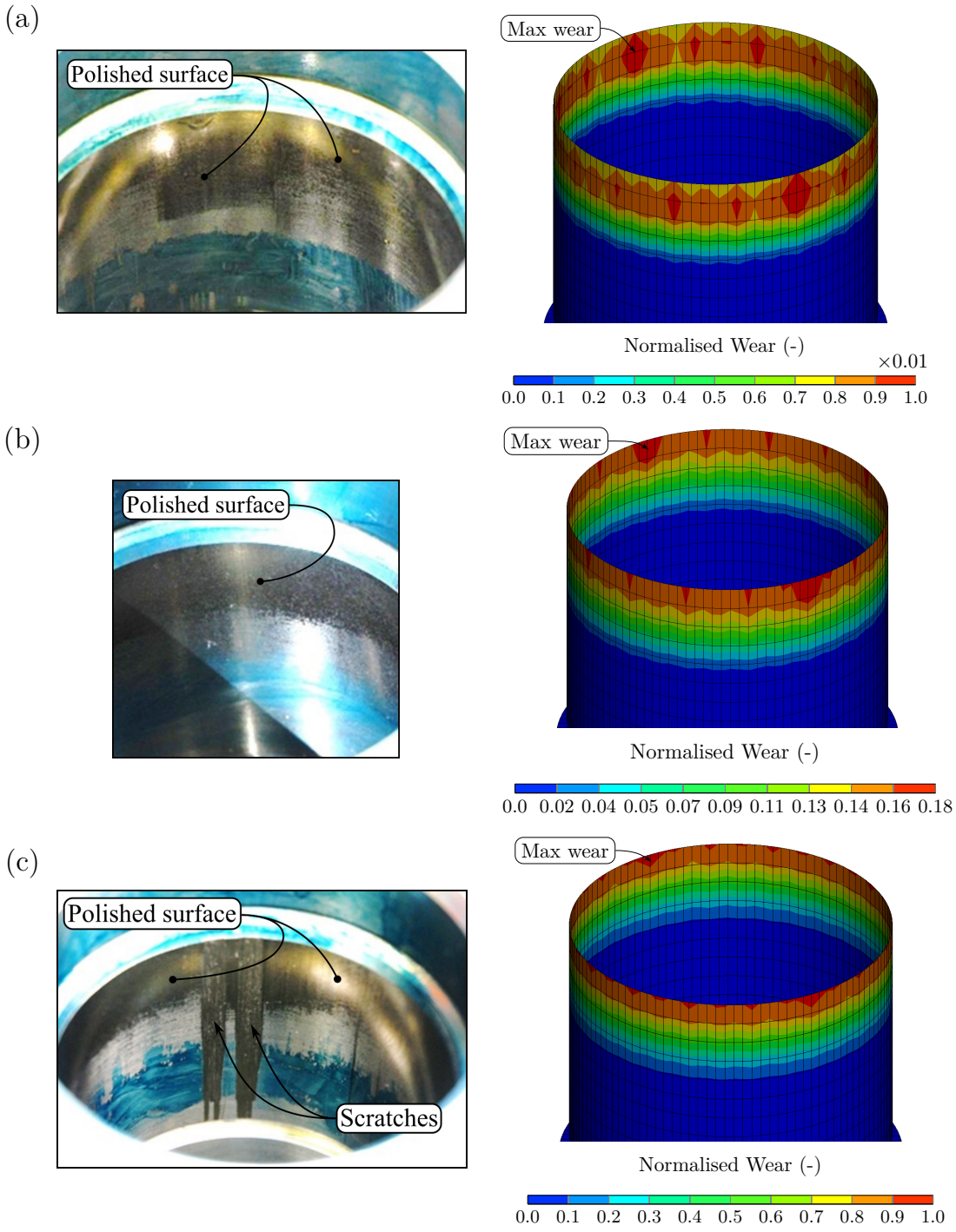

Figure 12. Results for the liner from the experiments and the corresponding simulations showing nodal results of the normalised total wear depth for (a) case 3, (b) case 4, and (c) case 5. Note that different fringe scales are present.

observed on the liner used in the experiment. For the piston, see Figure 13, the wear is concentrated to a narrow region around the circumference on the middle of the piston, i.e. at the lower part of the light grey surface in Figure 13a. The simulated

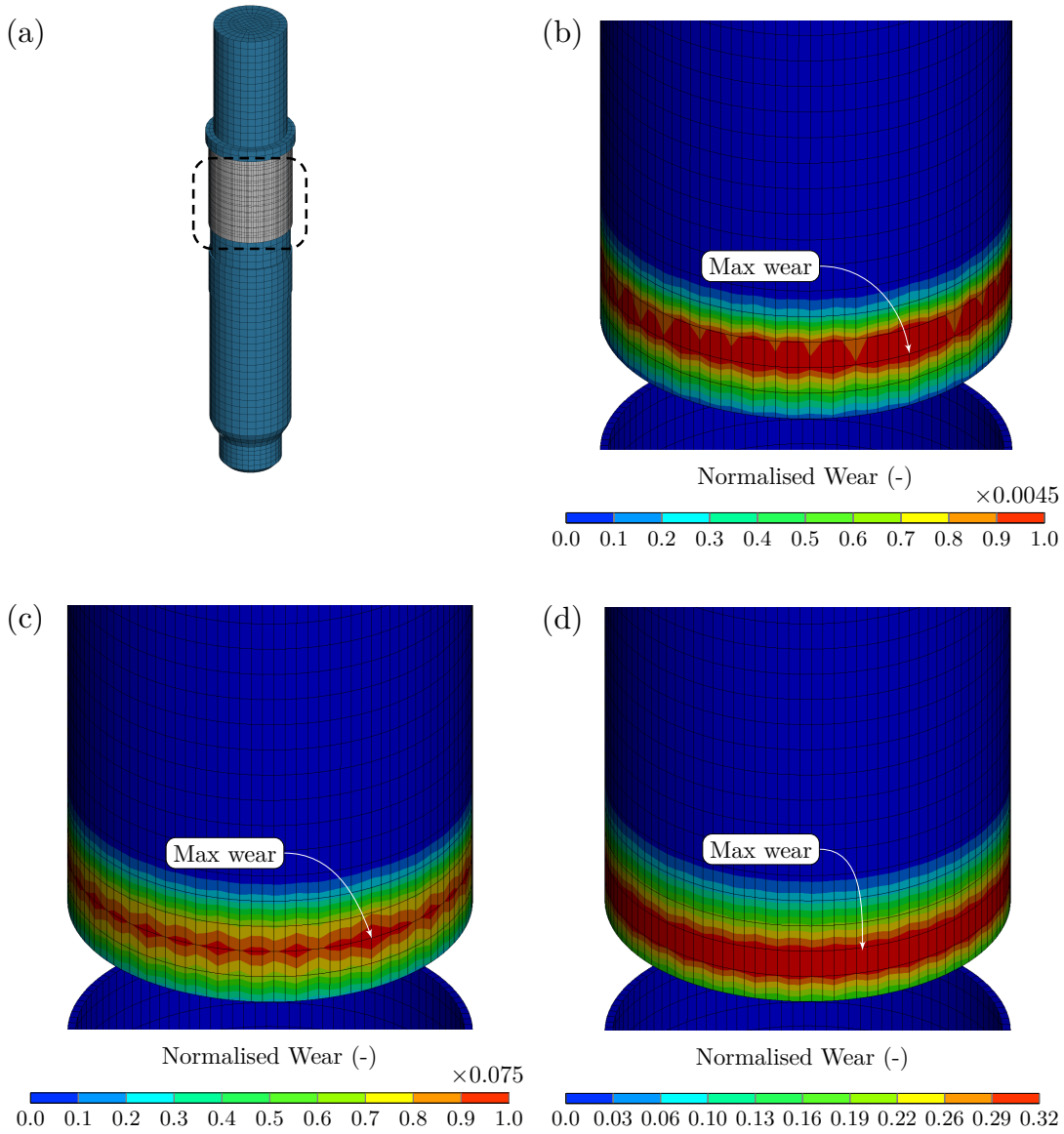

Figure 13. Simulation results for the light grey surface on the piston (a) showing nodal results of the normalised total wear depth for (b) case 3, (c) case 4, and (d) case 5. Note that different fringe scales are present.

normalised wear/cycle for case 3 and 4 for the piston are a factor ≈0.4 of the values for the liner. The main reason for the lower wear on the piston can be explained by its higher hardness. The picture from case 5, see Figure 12c, where the observed scratches clearly indicate that seizure has occurred, and thus also adhesive wear. The simulation of case 5 shows that the wear/cycle for the liner is approximately a factor of 5.4 larger than in case 4, and this level of simulated wear can be used as an indicator for seizure for this material combination. The wear/cycle for the piston is a factor ≈0.3 of the wear/cycle for the liner.

In this study, one type of operation where wear can occur in a hydraulic percussion unit has been simulated, and the results have been validated against an experimental testing program. The simulated results of wear depth and the observed results from

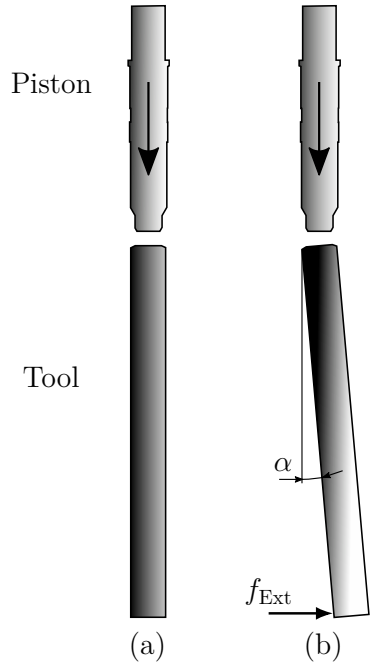

Figure 14. The standard straight impact (a) and the misaligned impact (b) between the piston and the tool, which in the latter case is misaligned by an angle α due to the external force f_{Ext}.

the experiment have a similar overall wear pattern. The goal of this work was to develop a method that could be used for predicting wear, and ultimately seizure, in percussion units. A good agreement between simulation and experimental results could be confirmed, hence the proposed simulation method should have the potential of predicting wear in such units.

4.1. Misaligned impact

In the previous section wear patterns for a perfectly straight impact have been simulated which must be considered as an idealistic condition that rarely occurs in real operation of percussion units. More realistically, the tool will often be misaligned to a certain degree due to the gap between the tool and the tool bushing, but also due to external lateral forces that arise in real work. Figure 14 shows an impact on a misaligned tool that is subjected to an external force. A versatile simulation tool for percussion units must be capable of simulating the response from many different running conditions to evaluate the robustness on virtual prototypes of such units. The condition of misaligned impacts should be one of the more important since it occurs regularly in real operation. Furthermore, it should be pointed out that no experiment has been carried out for the misaligned running condition and the simulation results in this section shall only be considered as a demonstration of capabilities of the simulation tool. In the replication of the experiment setup it was however well motivated to use a straight impact condition because the gap mentioned above was minimised and the external lateral forces that occur in the test rig are insignificant.

The gap for brand new components is determined by the design tolerances and the variances that occurs in the manufacturing, which will generate a misalignment angle α in the range of 0.1°–0.2°, see Figure 14. For used components that have been in

real operation in the field and that have been worn, larger gaps occur that make it possible for an increased radial movement of the tool and a misalignment up to 1°. The running condition of a misaligned tool generates radial forces and movements of the piston at impact, and may be a potential root cause for creating wear in the percussion unit, and most likely a more severe running condition from a wear damage perspective when compared to a straight ideal impacting condition. If the radial motion is large enough the piston will come into contact with the liner, and wear will arise when the piston is sliding against the liner. This situation can be compared to the cases 1–5 were the piston and the liner are concentric and contact is established by deformation of the liner. To demonstrate this running condition of a misaligned impact and the wear it generates, two simulation cases were defined, i.e. case 6 and 7, with an initial misalignment of 0.14° and 0.5° respectively. Case 6 is representing a condition of new components and case 7 the condition of worn components. These cases were simulated using the model from Section 3.2, but where the normalised operating pressure was set to 0.57 in relation to the average pressure $\overline{p}_{\mathrm{C}}$ for the running condition 5, which represents a normal running condition for a hydraulic percussion unit in real operation. The initial angle of misalignment was established by a rotation of the tool and the bushing prior to the simulation, rather than to apply an external force and adjusting the gap between the components. This procedure was used to reduce the fluctuation of the misalignment angle between each impact.

The simulated wear results are shown in Figure 15, and in general different wear patterns are generated in comparison to case 3–5, see Figure 12 and 13; the numerical values of the wear results are presented in Table 3. The regions of large wear are located at diametrically opposite positions, see the points P1–P2 and P3–P4 in Figure 15a and c, which originates from the radial movements of the piston that are induced by the misaligned impact. Because the tool was misaligned in a certain plane, the radial motion of the piston will follow this direction, and as a consequence the wear pattern will be located in the same plane. Due to the radial movements of the tool, which are excited at each impact, the angle of misalignment shows minor fluctuation around the initial value throughout the course of the simulation, i.e. $< \pm 0.006°$ for both cases.

The wear pattern for case 6, see Figure 15a, has different shapes on each side of the liner, see the results near by the points P1 and P2, but for case 7 the wear pattern is similar on each side, see Figure 15c. The lower wear depth at P2 for case 6 can be explained by the smaller misalignment, that causes smaller radial movements of the piston than for case 7. Further, the radial movements are dampened by the viscous forces of the oil film. The results for case 6 are showing a wear/cycle somewhat lower than for case 5 both for the liner and the piston, which should indicate that there is a low risk for seizure. On the other hand, the results for case 7 are showing larger wear/cycle for the liner than for case 5 even though the operating pressure is 0.43 times lower. However, the wear/cycle is on the same level for the piston, see Table 3. The wear/cycle for the liner was for case 7 estimated to 0.43, which is 1.73 times higher than for case 5, and should indicate high risk for seizure because the running condition 5 in the experiment resulted in such damage. However, the wear damage is

Table 3. Normalised simulation results from the misaligned impact.

Case	Misalignment α (°)	$\overline{p}_{\mathrm{C}}$ (-)	Max Δp (-)	Liner Wear/cycle	Piston Wear/cycle
6	0.14	0.57	0.54	0.09	0.032
7	0.5	0.57	0.54	0.43	0.081

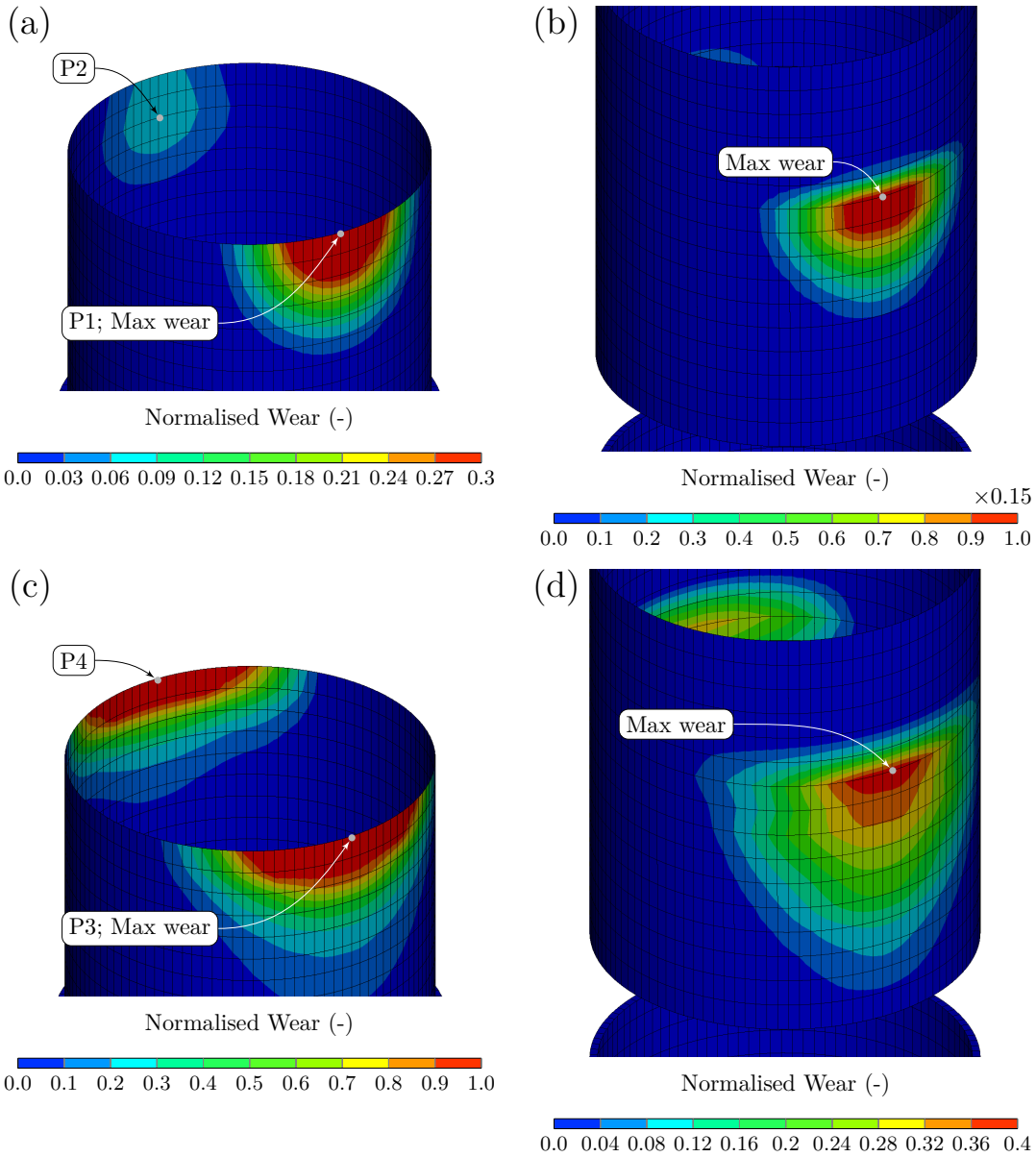

Figure 15. Results from the simulation of misaligned impact showing nodal results of the normalised total wear depth for case 6 (a) liner and (b) piston and for case 7 (c) liner and (d) piston. Two diametrically opposite points P1 and P2 for case 6 and P3 and P4 for case 7, where large wear have occurred, are indicated in (a) and (c).

more localised compared to case 5, compare the Figures 12 and 13 to Figure 15, and to validate if seizure actually occurs at the misaligned running condition, it is necessary to conduct an experiment for a corresponding running condition, which has not been done in this work and thus is a topic for further studies.

The accumulated wear for the two diametrically opposite points P1 and P2 for case 6, and for P3 and P4 for case 7 on the liner, which are where the maximum accumulated wear is registered, is shown in Figure 16. These curves have a different characteristic than for case 3–5, see Figure 11, and the main part of the wear for

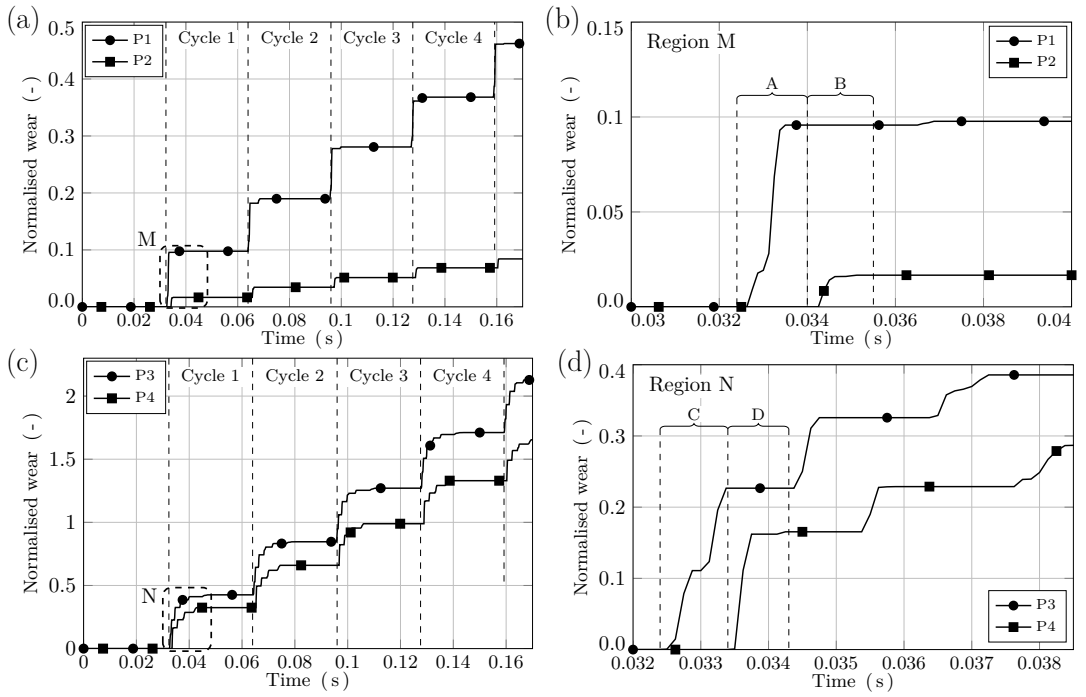

Figure 16. The normalised accumulated wear for the misaligned impact for the points P1–P4 on the liner. The regions M and N are displayed in a smaller scale (b) and (d) to present the differences in the generation of wear, where the phase A–D indicates typical behaviours, at each point.

each cycle occurs immediately after the impact. Furthermore, wear occurs first at the points P1 and P3 since the piston is moved against these points due to radial forces that are generated at impact, and then the piston is moved to the opposite side, and wear occurs at points P2 and P4. In case 3–5 the wear depth are generated in a more smooth manner over the return stroke for the piston, while for the misaligned impact a step wise generation of wear can be noticed. This behaviour can be explained by the radial movement of the piston that is induced by the misaligned impact, and by that the piston will bounce between the diametrically opposite points in the liner. While wear is generated at point P1, see phase A in Figure 16b, no wear is generated at point P2, i.e. the accumulated wear is fixed at a constant level, and when wear is generated at P2, see phase B, no wear occurs at P1. A similar behaviour can also be noticed for case 7, see phase C and D in Figure 16d, but here the magnitude is higher and the wear generation phases are more distinct, which can be related to the larger misalignment than for case 6. The wear for case 6 is generated at contact for only one or two occasions for each cycle, while contact occurs for a longer time period for case 7 during each working cycle. This different behaviour for case 6 and 7 can be explained by the level of misalignment and the effects of the oil film. The generated radial forces for case 6 are on a level that can be handled by the oil film to prevent contact, but for case 7 the forces are larger than what can be generated by the oil film, which may be analogous to a collapsing oil film, and contact will occur.

The simulated wear from the misaligned impact of case 7 is higher than in case 5, which already has been mentioned, however, there are some important differences in the loading of the contact surfaces between these cases that need to be considered. The piston motion from a misaligned impact seems to behave in a proper way physically,

but the structural contact between the piston and the liner is also very important when simulating wear. Here, this contact has been modelled by two parts, first the mechanical contact, and secondly the oil film, which is represented by the viscous fluid pressure that is generated when the fluid between the piston and liner is compressed. In case 3–5 a good agreement was found between the experiment and the simulations, and this would indicate that the modelling of the contact is good enough to represent the real mechanism. However, the generation of the contact forces for case 3–5 and for case 6 and 7 are very different. In case 3–5 the contact forces are ramped up in a smooth way due to the deformation of the liner, and the surfaces in contact are loaded uniformly around the circumference. In case 6 and 7, the contact surfaces are loaded by a short duration radial force, which originates from the radial impact from the piston. Further, the contact region is small, which is due to the cylindrical shape of the contact surfaces on the components, and that the surfaces not are fully parallel. Thus, the loading differs in a fundamental way, and the modelling of the structural contact, and especially the oil film, might need to be improved to be able to handle the more complex contact forces that occur for misaligned impact.

In this section, two running conditions of misaligned impacts have been simulated, and the overall responses give the idea of being realistic even though no experimental data are available for validation. Furthermore, the simulated wear patterns also give an impression of what can be expected in the real case. These results further emphasises the potential of the proposed method for predicting wear in hydraulic percussion units.

5. Concluding Remarks

In this work, a method for predicting wear in hydraulic percussion units is presented. The fundaments of this method are a co-simulation approach to simulate the main mechanisms and the structural responses of the percussion unit, and utilisation of the wear routines in LS-DYNA. The simulated results of wear have been compared against corresponding results from an experiment at straight impacting conditions. The wear pattern of the simulations and the experiment was found to correspond to a large extent.

The running condition of a misaligned impact has also been simulated, and the corresponding wear was calculated. This result is showing a realistic wear pattern, with a calculated wear depth that is significantly greater than for the straight condition. The validity of the wear depth results has not been further studied in this work, and to judge if these are reasonable more experiments need to be performed.

The most important contributions from this work are:

- the co-simulation approach was successfully utilised to study wear related mechanisms;
- the wear routines in LS-DYNA were applied to study the wear in percussion units with good utilisation in conjunction to the co-simulation procedure;
- the simulated wear for a misaligned impacting condition looked realistic, even though further modelling and experimental work are needed;
- the method has a potential for use as a virtual tool for designing against wear in future hydraulic percussion units.

Acknowledgement(s)

The authors would like to thank the project initiator Erik Sigfridsson and Epiroc Tools & Attachments Division for funding this study. Furthermore, Magnus Karlsson is greatly acknowledged for performing the experiment.

Disclosure statement

No potential conflict of interest was reported by the authors.

Nomenclature

Nomenclature

Abbreviations

FE	Finite Element
FMI	Functional Mock-up Interface
FMU	Functional Mock-up Unit

Subscripts

A	Cavity A
C	Cavity C
p	Piston
N	Co-simulation component index
Exp	Experiment

Variables

α	Angle
C	Clearance, m
$\dot{d}$	Sliding speed, m/s
e	Eccentric distance, m
f	Force, N
H	Hardness, Pa
h	Gap height, m
k	Wear coefficient, -
n, m	Index
p	Pressure, Pa
Q	Flow, m^3/s
s	Sliding distance, m
u	Displacement, m
$\mathbf{u}$	Displacement, vector, m
$\dot{u}$	Speed, m/s
V	Volume, m^3
W	Load, N
w	Wear depth, m
$\dot{w}$	Wear depth rate, m/s

References

[1] Park JW, Kim HE. Development of the test system for measuring the impact energy of a hydraulic breaker. Proceedings of the JFPS International Symposium on Fluid Power. 2005;2005(6):75–79.
[2] Lundberg B. Computer modeling and simulation of percussive drilling of rock; comprehensive rock engineering: Principles, practice and projects. Vol. 4. Pergamon Press; 1993.
[3] Giuffrida A, Laforgia D. Modelling and simulation of a hydraulic breaker. International Journal of Fluid Power. 2005;6(2):47–56.
[4] Ohmae N, Tsukizoe T. Analysis of a wear process using the finite element method. Wear. 1980;61(2):333–339.

[5] Põdra P, Andersson S. Simulating sliding wear with finite element method. Tribology international. 1999;32(2):71–81.
[6] Archard J. Contact and rubbing of flat surfaces. Journal of applied physics. 1953; 24(8):981–988.
[7] Borrvall T, Jernberg A, Schill M, et al. Simulation of wear processes in LS-DYNA. In: 14th International LS-DYNA Users Conference, June 12-14, 2016, Detroit, USA. Livermore Software Technology Corporation; 2016.
[8] LST. LS-DYNA R12 keyword user's manual. Livermore, USA: Livermore Software Technology; 2020.
[9] Puryear J, Reese L, Harrison B. Wear analysis of machinery components in buildings. In: 16th International LS-DYNA Users Conference, June 10-11, 2020, Virtual event. Livermore Software Technology Corporation; 2020.
[10] Hatam A, Khalkhali A. Simulation and sensitivity analysis of wear on the automotive brake pad. Simulation Modelling Practice and Theory. 2018;84:106 – 123.
[11] Andersson H, Nordin P, Borrvall T, et al. A co-simulation method for system-level simulation of fluid–structure couplings in hydraulic percussion units. Engineering with Computers. 2017 Apr;33(2):317–333.
[12] Andersson H, Simonsson K, Hilding D, et al. System level co-simulation of a control valve and hydraulic cylinder circuit in a hydraulic percussion unit. In: 15th Scandinavian International Conference on Fluid Power, June 7-9, 2017, Linköping, Sweden; Vol. 144; Linköping University Electronic Press; 2017. p. 225–235.
[13] Andersson H, Simonsson K, Hilding D, et al. Validation of a co-simulation approach for hydraulic percussion units applied to a hydraulic hammer. Advances in Engineering Software. 2019;131:102–115.
[14] Andersson H, Holmberg LJ, Simonsson K, et al. Simulation of leakage flow through dynamic sealing gaps in hydraulic percussion units using a co-simulation approach. Simulation Modelling Practice and Theory. 2021;111:102351.
[15] Blochwitz T, Otter M, Åkesson J, et al. Functional mockup interface 2.0: The standard for tool independent exchange of simulation models. In: Proceedings of the 9th International Modelica Conference; September; Munich, Germany; 2012. p. 173–184.
[16] Axin M, Braun R, Dell'Amico A, et al. Next generation simulation software using transmission line elements. In: Fluid Power and Motion Control, 15th-17th September, Bath, England, UK; Centre for Power Transmission and Motion Control; 2010. p. 265–276.
[17] Hutchings I, Shipway P. Tribology: friction and wear of engineering materials. Butterworth-Heinemann; 2017.